

Measurement of the D⁺-meson production cross section at low transverse momentum in p p collisions at $\sqrt{s}=1.96$ TeV

著者別名	原 和彦, 金 信弘, 佐藤 構二, 受川 史彦
journal or publication title	Physical review D
volume	95
number	9
page range	092006
year	2017-05
権利	(C) 2017 American Physical Society
URL	http://hdl.handle.net/2241/00146704

doi: 10.1103/PhysRevD.95.092006

Measurement of the D^+ -meson production cross section at low transverse momentum in $p\bar{p}$ collisions at $\sqrt{s} = 1.96$ TeV

T. Aaltonen,²¹ S. Amerio,^{39a,39b} D. Amidei,³¹ A. Anastassov,^{15,w} A. Annovi,¹⁷ J. Antos,¹² G. Apollinari,¹⁵ J. A. Appel,¹⁵ T. Arisawa,⁵¹ A. Artikov,¹³ J. Asaadi,⁴⁷ W. Ashmanskas,¹⁵ B. Auerbach,² A. Aurisano,⁴⁷ F. Azfar,³⁸ W. Badgett,¹⁵ T. Bae,²⁵ A. Barbaro-Galtieri,²⁶ V. E. Barnes,⁴³ B. A. Barnett,²³ P. Barria,^{41a,41c} P. Bartos,¹² M. Bauce,^{39a,39b} F. Bedeschi,^{41a} S. Behari,¹⁵ G. Bellettini,^{41a,41b} J. Bellinger,⁵³ D. Benjamin,¹⁴ A. Beretvas,¹⁵ A. Bhatti,⁴⁵ K. R. Bland,⁵ B. Blumenfeld,²³ A. Bocci,¹⁴ A. Bodek,⁴⁴ D. Bortoletto,⁴³ J. Boudreau,⁴² A. Boveia,¹¹ L. Brigliadori,^{6a,6b} C. Bromberg,³² E. Brucken,²¹ J. Budagov,¹³ H. S. Budd,⁴⁴ K. Burkett,¹⁵ G. Busetto,^{39a,39b} P. Bussey,¹⁹ P. Butti,^{41a,41b} A. Buzatu,¹⁹ A. Calamba,¹⁰ S. Camarda,⁴ M. Campanelli,²⁸ F. Canelli,^{11,ee} B. Carls,²² D. Carlsmith,⁵³ R. Carosi,^{41a} S. Carrillo,^{16,1} B. Casal,^{9,j} M. Casarsa,^{48a} A. Castro,^{6a,6b} P. Catastini,²⁰ D. Cauz,^{48a,48b,48c} V. Cavaliere,²² A. Cerri,^{26,e} L. Cerrito,^{28,r} Y. C. Chen,¹ M. Chertok,⁷ G. Chiarelli,^{41a} G. Chlachidze,¹⁵ K. Cho,²⁵ D. Chokheli,¹³ A. Clark,¹⁸ C. Clarke,⁵² M. E. Convery,¹⁵ J. Conway,⁷ M. Corbo,^{15,z} M. Cordelli,¹⁷ C. A. Cox,⁷ D. J. Cox,⁷ M. Cremonesi,^{41a} D. Cruz,⁴⁷ J. Cuevas,^{39a,39b} R. Culbertson,¹⁵ N. d'Ascenzo,^{15,v} M. Datta,^{15,hh} P. de Barbaro,⁴⁴ L. Demortier,⁴⁵ M. Deninno,^{6a} M. D'Errico,^{39a,39b} F. Devoto,²¹ A. Di Canto,^{41a,41b} B. Di Ruzza,^{15,p} J. R. Dittmann,⁵ S. Donati,^{41a,41b} M. D'Onofrio,²⁷ M. Dorigo,^{48a,48d} A. Driutti,^{48a,48b,48c} K. Ebina,⁵¹ R. Edgar,³¹ R. Erbacher,⁷ S. Errede,²² B. Esham,²² S. Farrington,³⁸ J. P. Fernández Ramos,²⁹ R. Field,¹⁶ G. Flanagan,^{15,t} R. Forrest,⁷ M. Franklin,²⁰ J. C. Freeman,¹⁵ H. Frisch,¹¹ Y. Funakoshi,⁵¹ C. Galloni,^{41a,41b} A. F. Garfinkel,⁴³ P. Garosi,^{41a,41c} H. Gerberich,²² E. Gerchtein,¹⁵ S. Giagu,^{46a} V. Giakoumopoulou,³ K. Gibson,⁴² C. M. Ginsburg,¹⁵ N. Giokaris,^{3,*} P. Giromini,¹⁷ V. Glagolev,¹³ D. Glenzinski,²⁹ M. Gold,³⁴ D. Goldin,⁴⁷ A. Golossanov,¹⁵ G. Gomez,⁹ G. Gomez-Ceballos,³⁰ M. Goncharov,³⁰ O. González López,²⁹ I. Gorelov,³⁴ A. T. Goshaw,¹⁴ K. Goulianos,⁴⁵ E. Gramellini,^{6a} C. Grosso-Pilcher,¹¹ J. Guimaraes da Costa,²⁰ S. R. Hahn,¹⁵ J. Y. Han,⁴⁴ F. Happacher,¹⁷ K. Hara,⁴⁹ M. Hare,⁵⁰ R. F. Harr,⁵² T. Harrington-Taber,^{15,m} K. Hatakeyama,⁵ C. Hays,³⁸ J. Heinrich,⁴⁰ M. Herndon,⁵³ A. Hocker,¹⁵ Z. Hong,⁴⁷ W. Hopkins,^{15,f} S. Hou,¹ R. E. Hughes,³⁵ U. Husemann,⁵⁴ M. Hussein,^{32,cc} J. Huston,³² G. Introzzi,^{41a,41e,41f} M. Iori,^{46a,46b} A. Ivanov,^{7,o} E. James,¹⁵ D. Jang,¹⁰ B. Jayatilaka,¹⁵ E. J. Jeon,²⁵ S. Jindariani,¹⁵ M. Jones,⁴³ K. K. Joo,²⁵ S. Y. Jun,¹⁰ T. R. Junk,¹⁵ M. Kambeitz,²⁴ T. Kamon,^{25,47} P. E. Karchin,⁵² A. Kashi,⁵ Y. Kato,^{37,n} W. Ketchum,^{11,ii} J. Keung,⁴⁰ B. Kilminster,^{15,ee} D. H. Kim,²⁵ H. S. Kim,^{15,bb} J. E. Kim,¹⁷ M. J. Kim,¹⁷ S. H. Kim,⁴⁹ S. B. Kim,²⁵ Y. J. Kim,²⁵ Y. K. Kim,¹¹ N. Kimura,⁵¹ M. Kirby,¹⁵ K. Kondo,^{51,*} D. J. Kong,²⁵ J. Konigsberg,¹⁶ A. V. Kotwal,¹⁴ M. Kreps,²⁴ J. Kroll,⁴⁰ M. Kruse,¹⁴ T. Kuhr,²⁴ M. Kurata,⁴⁹ A. T. Laasanen,⁴³ S. Lammel,¹⁵ M. Lancaster,²⁸ K. Lannon,^{35,x} G. Latino,^{41a,41c} H. S. Lee,²⁵ J. S. Lee,²⁵ S. Leo,²² S. Leone,^{41a} J. D. Lewis,¹⁵ A. Limosani,^{14,s} E. Lipeles,⁴⁰ A. Lister,^{18,a} Q. Liu,⁴³ T. Liu,¹⁵ S. Lockwitz,⁵⁴ A. Loginov,⁵⁴ D. Lucchesi,^{39a,39b} A. Lucà,¹⁷ J. Lueck,²⁴ P. Lujan,²⁶ P. Lukens,¹⁵ G. Lungu,⁴⁵ J. Lys,^{26,*} R. Lysak,^{12,d} R. Madrak,¹⁵ P. Maestro,^{41a,41c} S. Malik,⁴⁵ G. Manca,^{27,b} A. Manousakis-Katsikakis,³ L. Marchese,^{6a,jj} F. Margaroli,^{46a} P. Marino,^{41a,41d} K. Matera,²² M. E. Mattson,⁵² A. Mazzacane,¹⁵ P. Mazzanti,^{6a} R. McNulty,^{27,i} A. Mehta,²⁷ P. Mehtala,²¹ C. Mesropian,⁴⁵ T. Miao,¹⁵ D. Mietlicki,³¹ A. Mitra,¹ H. Miyake,⁴⁹ S. Moed,¹⁵ N. Moggi,^{6a} C. S. Moon,^{15,z} R. Moore,^{15,ff,gg} M. J. Morello,^{41a,41d} A. Mukherjee,¹⁵ Th. Muller,²⁴ P. Murat,¹⁵ M. Mussini,^{6a,6b} J. Nachtman,^{15,m} Y. Nagai,⁴⁹ J. Naganoma,⁵¹ I. Nakano,³⁶ A. Napier,⁵⁰ J. Nett,⁴⁷ T. Nigmanov,⁴² L. Nodulman,² S. Y. Noh,²⁵ O. Norriella,²² L. Oakes,³⁸ S. H. Oh,¹⁴ Y. D. Oh,²⁵ T. Okusawa,³⁷ R. Orava,²¹ L. Ortolan,⁴ C. Pagliarone,^{48a} E. Palencia,^{9,e} P. Palni,³⁴ V. Papadimitriou,¹⁵ W. Parker,⁵³ G. Pauletta,^{48a,48b,48c} M. Paulini,¹⁰ C. Paus,³⁰ T. J. Phillips,¹⁴ G. Piacentino,^{15,q} E. Pianori,⁴⁰ J. Pilot,⁷ K. Pitts,²² C. Plager,⁸ L. Pondrom,⁵³ S. Poprocki,^{15,f} K. Potamianos,²⁶ A. Pranko,²⁶ F. Prokoshin,^{13,aa} F. Ptohos,^{17,g} G. Punzi,^{41a,41b} I. Redondo Fernández,²⁹ P. Renton,³⁸ M. Rescigno,^{46a} F. Rimondi,^{6a,*} L. Ristori,^{41a,15} A. Robson,¹⁹ T. Rodriguez,⁴⁰ S. Rolli,^{50,h} M. Ronzani,^{41a,41b} R. Roser,¹⁵ J. L. Rosner,¹¹ F. Ruffini,^{41a,41c} A. Ruiz,⁹ J. Russ,¹⁰ V. Rusu,¹⁵ W. K. Sakumoto,⁴⁴ Y. Sakurai,⁵¹ L. Santi,^{48a,48b,48c} K. Sato,⁴⁹ V. Saveliev,^{15,v} A. Savoy-Navarro,^{15,z} P. Schlabach,¹⁵ E. E. Schmidt,¹⁵ T. Schwarz,³¹ L. Scodellaro,⁹ F. Scuri,^{41a} S. Seidel,³⁴ Y. Seiya,³⁷ A. Semenov,¹³ F. Sforza,^{41a,41b} S. Z. Shalhout,⁷ T. Shears,²⁷ P. F. Shepard,⁴² M. Shimojima,^{49,u} M. Shochet,¹¹ I. Shreyber-Tecker,³³ A. Simonenko,¹³ K. Sliwa,⁵⁰ J. R. Smith,⁷ F. D. Snider,¹⁵ H. Song,⁴² V. Sorin,⁴ R. St. Denis,^{19,*} M. Stancari,¹⁵ D. Stentz,^{15,w} J. Strologas,³⁴ Y. Sudo,⁴⁹ A. Sukhanov,¹⁵ I. Suslov,¹³ K. Takemasa,⁴⁹ Y. Takeuchi,⁴⁹ J. Tang,¹¹ M. Tecchio,³¹ P. K. Teng,¹ J. Thom,^{15,f} E. Thomson,⁴⁰ V. Thukral,⁴⁷ D. Toback,⁴⁷ S. Tokar,¹² K. Tollefson,³² T. Tomura,⁴⁹ D. Tonelli,^{15,e} S. Torre,¹⁷ D. Torretta,¹⁵ P. Totaro,^{39a} M. Trovato,^{41a,41d} F. Ukegawa,⁴⁹ S. Uozumi,²⁵ F. Vázquez,^{16,1} G. Velev,¹⁵ C. Vellidis,¹⁵ C. Vernieri,^{41a,41d} M. Vidal,⁴³ R. Vilar,⁹ J. Vizán,^{9,dd} M. Vogel,³⁴ G. Volpi,¹⁷ P. Wagner,⁴⁰ R. Wallny,^{15,j} S. M. Wang,¹ D. Waters,²⁸ W. C. Wester III,¹⁵ D. Whiteson,^{40,c} A. B. Wicklund,² S. Wilbur,⁷ H. H. Williams,⁴⁰ J. S. Wilson,³¹ P. Wilson,¹⁵ B. L. Winer,³⁵ P. Wittich,^{15,f} S. Wolbers,¹⁵ H. Wolfe,³⁵ T. Wright,³¹ X. Wu,¹⁸ Z. Wu,⁵ K. Yamamoto,³⁷ D. Yamato,³⁷ T. Yang,¹⁵ U. K. Yang,²⁵ Y. C. Yang,²⁵ W.-M. Yao,²⁶ G. P. Yeh,¹⁵ K. Yi,^{15,m} J. Yoh,¹⁵ K. Yorita,⁵¹ T. Yoshida,^{37,k} G. B. Yu,¹⁴ I. Yu,²⁵ A. M. Zanetti,^{48a} Y. Zeng,¹⁴ C. Zhou,¹⁴ and S. Zucchelli^{6a,6b}

(CDF Collaboration)

- ¹*Institute of Physics, Academia Sinica, Taipei, Taiwan 11529, Republic of China*
²*Argonne National Laboratory, Argonne, Illinois 60439, USA*
³*University of Athens, 157 71 Athens, Greece*
⁴*Institut de Física d'Altes Energies, ICREA, Universitat Autònoma de Barcelona, E-08193 Bellaterra (Barcelona), Spain*
⁵*Baylor University, Waco, Texas 76798, USA*
^{6a}*Istituto Nazionale di Fisica Nucleare Bologna, I-40127 Bologna, Italy*
^{6b}*University of Bologna, I-40127 Bologna, Italy*
⁷*University of California, Davis, Davis, California 95616, USA*
⁸*University of California, Los Angeles, Los Angeles, California 90024, USA*
⁹*Instituto de Física de Cantabria, CSIC-University of Cantabria, 39005 Santander, Spain*
¹⁰*Carnegie Mellon University, Pittsburgh, Pennsylvania 15213, USA*
¹¹*Enrico Fermi Institute, University of Chicago, Chicago, Illinois 60637, USA*
¹²*Comenius University, 842 48 Bratislava, Slovakia; Institute of Experimental Physics, 040 01 Kosice, Slovakia*
¹³*Joint Institute for Nuclear Research, RU-141980 Dubna, Russia*
¹⁴*Duke University, Durham, North Carolina 27708, USA*
¹⁵*Fermi National Accelerator Laboratory, Batavia, Illinois 60510, USA*
¹⁶*University of Florida, Gainesville, Florida 32611, USA*
¹⁷*Laboratori Nazionali di Frascati, Istituto Nazionale di Fisica Nucleare, I-00044 Frascati, Italy*
¹⁸*University of Geneva, CH-1211 Geneva 4, Switzerland*
¹⁹*Glasgow University, Glasgow G12 8QQ, United Kingdom*
²⁰*Harvard University, Cambridge, Massachusetts 02138, USA*
²¹*Division of High Energy Physics, Department of Physics, University of Helsinki, FIN-00014, Helsinki, Finland;*
Helsinki Institute of Physics, FIN-00014 Helsinki, Finland
²²*University of Illinois, Urbana, Illinois 61801, USA*
²³*The Johns Hopkins University, Baltimore, Maryland 21218, USA*
²⁴*Institut für Experimentelle Kernphysik, Karlsruhe Institute of Technology, D-76131 Karlsruhe, Germany*
²⁵*Center for High Energy Physics: Kyungpook National University, Daegu 702-701, Korea;*
Seoul National University, Seoul 151-742, Korea;
Sungkyunkwan University, Suwon 440-746, Korea;
Korea Institute of Science and Technology Information, Daejeon 305-806, Korea;
Chonnam National University, Gwangju 500-757, Korea;
Chonbuk National University, Jeonju 561-756, Korea;
Ewha Womans University, Seoul 120-750, Korea
²⁶*Ernest Orlando Lawrence Berkeley National Laboratory, Berkeley, California 94720, USA*
²⁷*University of Liverpool, Liverpool L69 7ZE, United Kingdom*
²⁸*University College London, London WC1E 6BT, United Kingdom*
²⁹*Centro de Investigaciones Energéticas Medioambientales y Tecnológicas, E-28040 Madrid, Spain*
³⁰*Massachusetts Institute of Technology, Cambridge, Massachusetts 02139, USA*
³¹*University of Michigan, Ann Arbor, Michigan 48109, USA*
³²*Michigan State University, East Lansing, Michigan 48824, USA*
³³*Institution for Theoretical and Experimental Physics, ITEP, Moscow 117259, Russia*
³⁴*University of New Mexico, Albuquerque, New Mexico 87131, USA*
³⁵*The Ohio State University, Columbus, Ohio 43210, USA*
³⁶*Okayama University, Okayama 700-8530, Japan*
³⁷*Osaka City University, Osaka 558-8585, Japan*
³⁸*University of Oxford, Oxford OX1 3RH, United Kingdom*
^{39a}*Istituto Nazionale di Fisica Nucleare, Sezione di Padova, I-35131 Padova, Italy*
^{39b}*University of Padova, I-35131 Padova, Italy*
⁴⁰*University of Pennsylvania, Philadelphia, Pennsylvania 19104, USA*
^{41a}*Istituto Nazionale di Fisica Nucleare Pisa, I-56127 Pisa, Italy*
^{41b}*University of Pisa, I-56127 Pisa, Italy*
^{41c}*University of Siena, I-56127 Pisa, Italy*
^{41d}*Scuola Normale Superiore, I-56127 Pisa, Italy*
^{41e}*INFN Pavia, I-27100 Pavia, Italy*
^{41f}*University of Pavia, I-27100 Pavia, Italy*
⁴²*University of Pittsburgh, Pittsburgh, Pennsylvania 15260, USA*
⁴³*Purdue University, West Lafayette, Indiana 47907, USA*

- ⁴⁴University of Rochester, Rochester, New York 14627, USA
⁴⁵The Rockefeller University, New York, New York 10065, USA
^{46a}Istituto Nazionale di Fisica Nucleare, Sezione di Roma 1, I-00185 Roma, Italy
^{46b}Sapienza Università di Roma, I-00185 Roma, Italy
⁴⁷Mitchell Institute for Fundamental Physics and Astronomy, Texas A&M University, College Station, Texas 77843, USA
^{48a}Istituto Nazionale di Fisica Nucleare Trieste, I-34127 Trieste, Italy
^{48b}Gruppo Collegato di Udine, I-33100 Udine, Italy
^{48c}University of Udine, I-33100 Udine, Italy
^{48d}University of Trieste, I-34127 Trieste, Italy
⁴⁹University of Tsukuba, Tsukuba, Ibaraki 305, Japan
⁵⁰Tufts University, Medford, Massachusetts 02155, USA
⁵¹Waseda University, Tokyo 169, Japan
⁵²Wayne State University, Detroit, Michigan 48201, USA
⁵³University of Wisconsin-Madison, Madison, Wisconsin 53706, USA
⁵⁴Yale University, New Haven, Connecticut 06520, USA
(Received 31 October 2016; published 30 May 2017)

We report on a measurement of the D^+ -meson production cross section as a function of transverse momentum (p_T) in proton-antiproton ($p\bar{p}$) collisions at 1.96 TeV center-of-mass energy, using the full data set collected by the Collider Detector at Fermilab in Tevatron Run II and corresponding to 10 fb^{-1} of integrated luminosity. We use $D^+ \rightarrow K^- \pi^+ \pi^+$ decays fully reconstructed in the central rapidity region $|y| < 1$ with transverse momentum down to 1.5 GeV/ c , a range previously unexplored in $p\bar{p}$ collisions. Inelastic $p\bar{p}$ -scattering events are selected online using minimally biasing requirements followed by an optimized offline selection. The $K^- \pi^+ \pi^+$ mass distribution is used to identify the D^+ signal, and the D^+

*Deceased.

^aUniversity of British Columbia, Vancouver, BC V6T 1Z1, Canada.

^bIstituto Nazionale di Fisica Nucleare, Sezione di Cagliari, 09042 Monserrato (Cagliari), Italy.

^cUniversity of California Irvine, Irvine, CA 92697, USA.

^dInstitute of Physics, Academy of Sciences of the Czech Republic, 182 21, Czech Republic.

^eCERN, CH-1211 Geneva, Switzerland.

^fCornell University, Ithaca, NY 14853, USA.

^gUniversity of Cyprus, Nicosia CY-1678, Cyprus.

^hOffice of Science, U.S. Department of Energy, Washington, DC 20585, USA.

ⁱUniversity College Dublin, Dublin 4, Ireland.

^jETH, 8092 Zürich, Switzerland.

^kUniversity of Fukui, Fukui City, Fukui Prefecture, Japan 910-0017.

^lUniversidad Iberoamericana, Lomas de Santa Fe, México, C.P. 01219, Distrito Federal.

^mUniversity of Iowa, Iowa City, IA 52242, USA.

ⁿKinki University, Higashi-Osaka City, Japan 577-8502.

^oKansas State University, Manhattan, KS 66506, USA.

^pBrookhaven National Laboratory, Upton, NY 11973, USA.

^qIstituto Nazionale di Fisica Nucleare, Sezione di Lecce, Via Arnesano, I-73100 Lecce, Italy.

^rQueen Mary, University of London, London, E1 4NS, United Kingdom.

^sUniversity of Melbourne, Victoria 3010, Australia.

^tMuons, Inc., Batavia, IL 60510, USA.

^uNagasaki Institute of Applied Science, Nagasaki 851-0193, Japan.

^vNational Research Nuclear University, Moscow 115409, Russia.

^wNorthwestern University, Evanston, IL 60208, USA.

^xUniversity of Notre Dame, Notre Dame, IN 46556, USA.

^yUniversidad de Oviedo, E-33007 Oviedo, Spain.

^zCNRS-IN2P3, Paris, F-75205 France.

^{aa}Universidad Tecnica Federico Santa Maria, 110v Valparaiso, Chile.

^{bb}Sejong University, Seoul 143-747, Korea.

^{cc}The University of Jordan, Amman 11942, Jordan.

^{dd}Universite catholique de Louvain, 1348 Louvain-La-Neuve, Belgium.

^{ee}University of Zürich, 8006 Zürich, Switzerland.

^{ff}Massachusetts General Hospital, Boston, MA 02114 USA.

^{gg}Harvard Medical School, Boston, MA 02114 USA.

^{hh}Hampton University, Hampton, VA 23668, USA.

ⁱⁱLos Alamos National Laboratory, Los Alamos, NM 87544, USA.

^{jj}Università degli Studi di Napoli Federico II, I-80138 Napoli, Italy.

transverse impact-parameter distribution is used to separate prompt production, occurring directly in the hard-scattering process, from secondary production from b -hadron decays. We obtain a prompt D^+ signal of 2950 candidates corresponding to a total cross section $\sigma(D^+, 1.5 < p_T < 14.5 \text{ GeV}/c, |y| < 1) = 71.9 \pm 6.8(\text{stat}) \pm 9.3(\text{syst}) \mu\text{b}$. While the measured cross sections are consistent with theoretical estimates in each p_T bin, the shape of the observed p_T spectrum is softer than the expectation from quantum chromodynamics. The results are unique in $p\bar{p}$ collisions and can improve the shape and uncertainties of future predictions.

DOI: 10.1103/PhysRevD.95.092006

Measurements of cross sections for the production of hadrons containing bottom or charm quarks (heavy flavors) in hadron collisions offer fundamental information to test and refine phenomenological models of the strong interaction at small momentum transfer, a regime in which perturbative expansions are challenging. In addition, in searches for astrophysical neutrinos, knowledge of charm production cross sections has been demonstrated [1] to improve estimates for background rates from neutrinos produced in decays of charm hadrons from cosmic-ray interactions with atmospheric nuclei.

The first studies of heavy-flavor production performed at the Tevatron proton-antiproton ($p\bar{p}$) collider in 1992–1996 [2] yielded cross sections significantly larger than the predicted values [3] and prompted a dedicated effort in refining calculations [4], which resulted in reduced discrepancies. The program continued during Tevatron Run II (2001–2011), including first measurements of charm-meson cross sections using $p\bar{p}$ collisions at center-of-mass energy $\sqrt{s} = 1.96 \text{ TeV}$ [5]. Since 2010, CERN’s LHC pp collider has replaced the Tevatron as the most prolific charm-meson source, allowing the ALICE and LHCb experiments to report measurements of charm cross sections at $\sqrt{s} = 2.76\text{--}13.00 \text{ TeV}$ [6].

Measurements based on $p\bar{p}$ collisions, and probing different collision energies, remain essential to extend the understanding of QCD, because differing admixtures of parton-level processes contribute at different energies and initial states. Previous measurements in $p\bar{p}$ collisions [5] were restricted to mesons with transverse momentum $p_T > 6.0 \text{ GeV}/c$ because of the transverse-momentum thresholds used in the online event selection (trigger). The transverse momentum is the momentum component in the plane transverse to the beam. Extending the reach to lower p_T , hence further into the nonperturbative regime, provides novel and unique constraints to improve QCD phenomenological models.

In this paper, we report on a measurement of the production cross section for D^+ mesons down to $1.5 \text{ GeV}/c$ p_T , a range unexplored in $p\bar{p}$ collisions, and unlikely to be explored in the foreseeable future with this initial state. The measurement is performed as a function of meson transverse momentum using $D^+ \rightarrow K^-\pi^+\pi^+$ decays reconstructed in the full CDF Run II data set,

corresponding to 10 fb^{-1} of integrated luminosity. Throughout this paper, charge-conjugate decays are implied. Candidate D^+ signal events are selected from a minimum-bias sample, collected by imposing minimal requirements on the event features in order to minimize biases on the physics properties of charm decays. Events are divided into independent subsamples (p_T bins) according to the D^+ candidate p_T . In each, we apply a data-driven optimization of the offline selection and perform a two-dimensional simultaneous fit of the resulting distributions of the $K^-\pi^+\pi^+$ mass and D^+ impact parameter, defined as the minimum transverse distance between a particle’s trajectory and the beam. The fit determines, for each p_T bin, the prompt D^+ yield (D^+ mesons directly produced in the $p\bar{p}$ interaction or originating from charm resonances) by statistically subtracting secondary D^+ candidates (D^+ mesons originating from b -hadron decays). Each prompt yield is combined with the corresponding reconstruction and selection efficiencies, derived using simulation, to determine the cross section,

$$\sigma_i = \frac{N_i/2}{\int \mathcal{L} dt \cdot \epsilon_i \cdot \mathcal{B}}, \quad (1)$$

where N_i is the observed number of prompt D^+ and D^- mesons in the i th p_T bin. The factor $1/2$ is included because both D^+ and D^- mesons contribute to N_i and we report results solely for D^+ , assuming charge-symmetric production of charm quarks in the strong $p\bar{p}$ interaction. The integrated luminosity $\int \mathcal{L} dt$ is normalized to an inelastic cross section of $\sigma_{p\bar{p}} = 60.7 \pm 2.4 \text{ mb}$ [7], and ϵ_i is the global detection, reconstruction, and selection efficiency. The branching fraction used for the $D^+ \rightarrow K^-\pi^+\pi^+$ decay is $\mathcal{B} = (9.46 \pm 0.24)\%$ [8].

The CDF II detector is a multipurpose magnetic spectrometer surrounded by calorimeters and muon detectors [9]. It is roughly cylindrically symmetric around the beams and is described in a cylindrical coordinate system with the z axis along the incident proton beam direction. The detector components relevant for this analysis are as follows. A silicon microstrip vertex detector and a cylindrical open-cell drift chamber immersed in a nearly uniform 1.4 T axial magnetic field allow the reconstruction of charged-particle trajectories (tracks) in the pseudorapidity

range $|\eta| < 1$. The vertex detector contains seven concentric layers of single- and double-sided silicon sensors at radii between 1.5 and 22 cm, each providing a position measurement with up to 15 (70) μm resolution in the azimuthal (longitudinal) direction [10]. The drift chamber has 96 measurement layers, located between 40 and 137 cm in radius, organized into alternating axial and $\pm 2^\circ$ stereo superlayers [11]. The transverse momentum is determined with a resolution of $\sigma_{p_T}/p_T^2 \approx 0.07\%$ $(\text{GeV}/c)^{-1}$, corresponding to a typical mass resolution of $6.0 \text{ MeV}/c^2$ for a $D^+ \rightarrow K^-\pi^+\pi^+$ decay. Gas Cherenkov detectors (CLC) covering the symmetric regions at a small polar angle around the interaction region $3.7 < |\eta| < 4.7$ are used to detect hard-scatter interactions and measure luminosity [12]. CDF has a three-level trigger system. We use events collected by the zero- and minimum-bias triggers, which are designed to collect events while introducing minimal bias in the properties of the particles produced in the collision. The zero-bias trigger applies no selection requirements and accepts a 10^{-6} fraction (prescale factor) of $p\bar{p}$ crossings, randomly chosen. At the first trigger level, the minimum-bias trigger accepts a 10^{-5} prescale fraction of the events in which a time coincidence between signals in the CLC at opposite sides of the interaction region is detected, which enriches the sample in $p\bar{p}$ crossings that yield inelastic interactions. At the second (third) trigger level, the minimum-bias trigger applies no requirements and accepts events with 3 (1) Hz maximum rates. The large prescale factors and accept-rate reductions avoid saturation of the data-writing rate. The resulting samples contain 183 million zero-bias and 133 million minimum-bias events. Of these, 409 events are common to both samples and used only once in the analysis.

The offline reconstruction of $D^+ \rightarrow K^-\pi^+\pi^+$ candidates is based solely on tracking information without using particle identification. The same-charge particles are assigned the pion mass. Three good-quality tracks, associated with drift-chamber and silicon-detector information and consistent with a $K^-\pi^+\pi^+$ decay, are combined in a kinematic fit to a common decay vertex to form a D^+ signal candidate. Additional selection criteria are applied on the vertex-fit quality; the minimum azimuthal separation of any pair of signal tracks; the product of their impact parameters; and the minimum value of D^+ transverse decay length projected onto the direction of its p_T , L_{xy} . These criteria are fully efficient for signal and reduce backgrounds from combinations of random charged particles (combinatorics). No events are observed with more than one reconstructed candidate. We further improve the signal-to-background ratio by optimizing the selection, separately for events restricted to each of the five D^+ candidate p_T bins, 1.5–2.5, 2.5–3.5, 3.5–4.5, 4.5–6.5, and 6.5–14.5 GeV/c . First, we apply an upper threshold of $100 \mu\text{m}$ on the impact parameter of the D^+ candidates. This suppresses secondary D^+ candidates, which are less likely to point back to the $p\bar{p}$

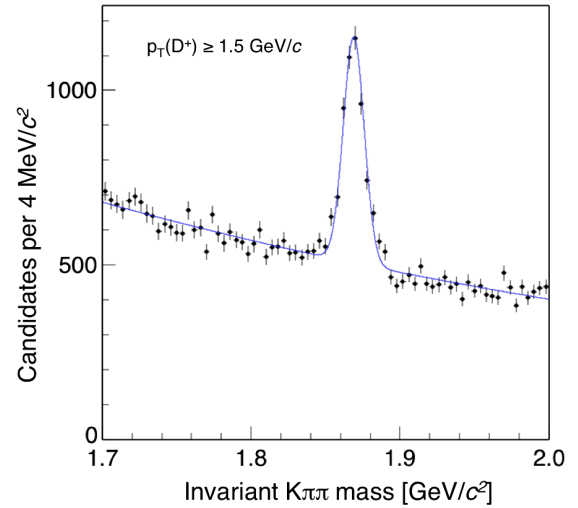


FIG. 1. Distribution of $K^-\pi^+\pi^+$ mass for the whole sample with the fit overlaid.

vertex because of the combined effect of the long lifetime of b hadrons and the energy released in their decay. This requirement is applied only for the optimization (see below) but is lifted in further analysis, where a fit of the D^+ impact-parameter distribution separates statistically the signal of prompt D^+ candidates from the secondaries. Then, we divide the sample randomly into two subsamples. In each, we conduct an independent optimization by maximizing the quantity $S/\sqrt{S+B}$ over 1000 possible configurations of requirements on the minimum p_T ($p_{T,\min}$) of any two final-state particles, minimum L_{xy} , and maximum value of the vertex-fit χ^2 . The signal (background) yields S (B) are estimated from fits of the $K^-\pi^+\pi^+$ mass distributions with a Gaussian model for the signal and a smooth empirical function for the background. Finally, the optimal configuration resulting from each subsample is applied on the complementary subsample. The use of a data-driven optimization avoids the modeling uncertainties of simulation-driven methods. Biases due to statistical fluctuations are avoided by applying selection criteria identified on one subsample to the other half of the sample. The optimized criteria vary in the ranges $p_{T,\min} > 0.6\text{--}1.1 \text{ GeV}/c$, $L_{xy} > 600\text{--}700 \mu\text{m}$, and $\chi^2 < 2\text{--}7$, depending on the subsample and p_T bin. The $K^-\pi^+\pi^+$ mass distribution of the resulting sample, summed over the full p_T range, is shown in Fig. 1. A prominent narrow peak of approximately 3400 $D^+ \rightarrow K^-\pi^+\pi^+$ decays, comprising both prompt signal and secondary charm candidates, overlaps a smooth background dominated by combinatorics. In each p_T bin, we determine the yield of prompt D^+ decays using a simultaneous maximum-likelihood fit to the unbinned distributions of $K^-\pi^+\pi^+$ mass, to separate D^+ decays from combinatorics, and D^+ impact parameter, to separate prompt from secondary D^+ decays. The fit model is a linear combination of probability density functions

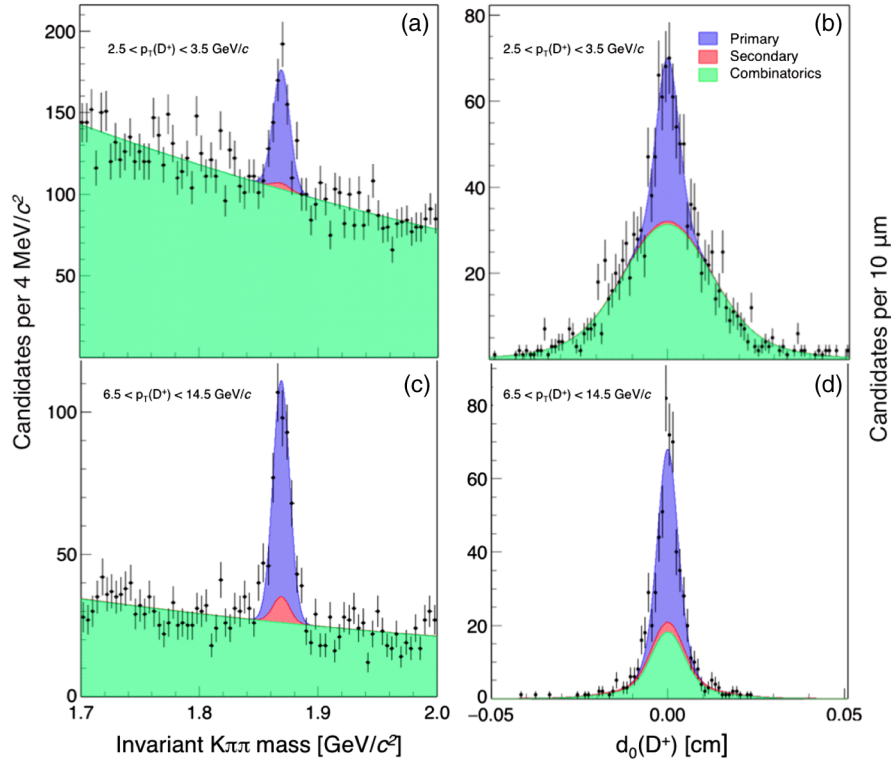


FIG. 2. Distributions of (a) the $K^-\pi^+\pi^+$ mass for candidates with $2.5 < p_T < 3.5$ GeV/ c and (b) the D^+ impact parameter for those candidates, further restricted to have $K^-\pi^+\pi^+$ mass within three standard deviations from the peak value. Fits are overlaid. Panels (c) and (d) show the same distributions for candidates with $6.5 < p_T < 14.5$ GeV/ c .

(PDFs) for a prompt D^+ signal, secondary D^+ , and combinatorial background, each consisting of the product of mass and impact-parameter PDFs. In the mass PDF, prompt and secondary components are modeled jointly with a Gaussian function determined from simulation; the background PDF is a second-order polynomial function derived empirically from regions with D^+ mass in 1.7–1.8 or 1.9–2.0 GeV/ c^2 (sidebands). In the impact-parameter PDF, the prompt (secondary) component is modeled with the sum of three narrow (broad) Gaussian distributions determined using simulation, whereas the background is modeled with a combination of Gaussian shapes that empirically reproduce the impact-parameter distribution of sideband events. The only free parameters in the fit are the numbers of prompt D^+ (signal) decays and secondary D^+ decays. Tests on simplified simulated experiments show that the fit estimates are unbiased and have proper Gaussian uncertainties. Figure 2 shows examples of fits in two p_T bins, $2.5 < p_T < 3.5$ GeV/ c and $6.5 < p_T < 14.5$ GeV/ c . A total signal of approximately 2950 prompt D^+ decays is obtained. The observed fraction of secondary decays is typically 15% of the total D^+ yield but ranges between 0% and 40% with large uncertainties, depending on p_T . We vary the signal and background models, and their parameters, and attribute systematic uncertainties on prompt-signal yields accordingly. The uncertainties associated with the impact-parameter model,

resulting from individual variations of primary, secondary, and background shapes, are in the range 0.9%–1.5%, depending on the candidate p_T . These dominate over the 0.10%–0.3% variations associated with the mass resolution-shape model.

We factorize the reconstruction efficiency ϵ_i , relative to the i th p_T bin, into the product of the trigger efficiency, the offline efficiency for reconstructing three tracks that meet the quality and fiducial requirements in the drift chamber, the offline efficiency for assigning the information from the silicon detector to these tracks, and the efficiency of the offline selection requirements. The zero-bias trigger efficiency is 100% by construction. The minimum-bias trigger efficiency is determined to be $(98.8_{-0.4}^{+0.2})\%$ from the ratio of D^+ signal yields observed in zero-bias events that meet, or fail, the minimum-bias requirements. All offline efficiencies are known to be reproduced accurately by the simulation [13] except for the term associated with the silicon detector. We therefore use efficiencies derived from simulation as inputs for the measurement and use control samples of data to obtain systematic uncertainties that cover potential data-simulation discrepancies in the silicon-related efficiency. Offline efficiencies ranging from 0.27% to 7.5% are determined from simulated events containing $D^+ \rightarrow K^-\pi^+\pi^+$ decays, in which distributions are weighted so that the multiplicity of prompt vertices reproduces the distribution observed in data. Control

TABLE I. Prompt D^+ -meson cross section results. All cross section values are integrated over the range $|y| < 1$. The second column (“effective p_T ”) lists the p_T values at which the differential cross section equals its average over that p_T bin, as determined using Ref. [14]. Values in the third (fourth) column are averaged (integrated) over each p_T bin. The first contribution to the uncertainties is statistical, and the second is systematic.

p_T range (GeV/c)	Eff. p_T (GeV/c)	$d\sigma(D^+, y < 1)/dp_T$ ($\mu\text{b}/\text{GeV}/c$)	$\sigma_i(D^+, y < 1)$ (μb)
1.5–2.5	2.04	$32.7 \pm 6.5 \pm 4.2$	$32.7 \pm 6.5 \pm 4.2$
2.5–3.5	2.98	$20.6 \pm 1.8 \pm 2.7$	$20.6 \pm 1.8 \pm 2.7$
3.5–4.5	3.97	$9.5 \pm 0.8 \pm 1.2$	$9.5 \pm 0.8 \pm 1.2$
4.5–6.5	5.38	$3.2 \pm 0.3 \pm 0.4$	$6.5 \pm 0.5 \pm 0.8$
6.5–14.5	9.19	$0.34 \pm 0.03 \pm 0.04$	$2.69 \pm 0.22 \pm 0.35$

samples of muons from $J/\psi \rightarrow \mu^+\mu^-$ decays and low-momentum pions from $D^{*+} \rightarrow D^0(\rightarrow K^-\pi^+)\pi^+$ decays, in which only drift-chamber information is used to select and reconstruct the charged particle, are used to determine silicon efficiencies as functions of charged-particle p_T and data-taking time from the fraction of charged particles that also meet the silicon requirements. The results are compared with silicon efficiencies determined in simulation, and the maximum observed deviation, 3.7%, is used as the systematic uncertainty on the per-track efficiency, resulting in an 11.5% uncertainty common to all D^+ transverse-momentum bins. This is the largest systematic uncertainty. Additional systematic uncertainties associated with imperfect descriptions of multitrack efficiency correlations, ionization energy loss, and hadronic interactions in the inner tracker material are negligible. Repeating the measurement on independent subsamples of data split according to data-taking time and the D candidate charge shows no evidence of residual biases.

The measured differential cross sections, averaged over each p_T bin and integrated over the rapidity range $|y| < 1$, are shown in Table I and displayed in Fig. 3. The observed cross sections are compatible with those predicted in recent calculations [14] and with those determined in early Run II using an independent data set [5]. The total cross section for the production of D^+ mesons in the kinematic range $1.5 < p_T < 14.5$ GeV/c and $|y| < 1$, obtained by summing over all p_T bins, is $71.9 \pm 6.8 \pm 9.3$ μb , where the first contribution to the uncertainty is statistical and the second is systematic.

In summary, we report on a measurement of the prompt D^+ -meson production cross section, as a function of transverse momentum, in proton-antiproton collisions at $\sqrt{s} = 1.96$ TeV, using the full data set collected by the CDF experiment in Tevatron Run II, and corresponding to 10 fb $^{-1}$ of integrated luminosity. We use prompt $D^+ \rightarrow K^-\pi^+\pi^+$ decays with transverse momenta down to 1.5 GeV/c fully reconstructed in the central rapidity region $|y| < 1$. The differential cross section is averaged in

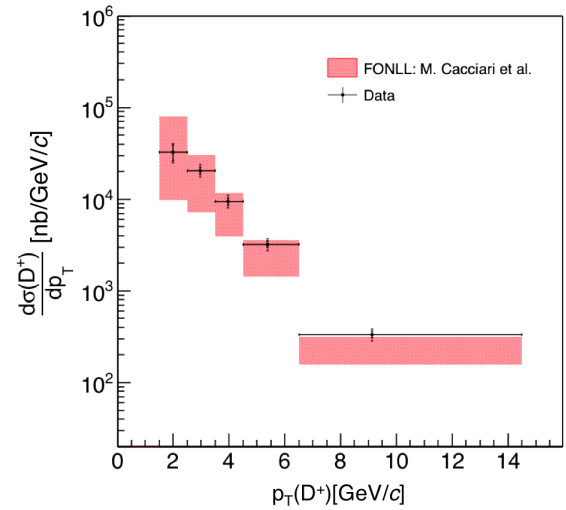


FIG. 3. Differential cross section as a function of p_T for prompt D^+ mesons with $p_T > 1.5$ GeV/c, compared with predictions from Ref. [14]. In each bin, the data point is displayed at the p_T value at which the differential cross section equals its average over that p_T bin, as determined using predictions from Ref. [14]. These “effective p_T ” values are also listed in Table I.

each p_T bin and integrated over the D^+ rapidity interval $|y| < 1$. The total cross section is $\sigma(D^+, 1.5 < p_T < 14.5 \text{ GeV}/c, |y| < 1) = 71.9 \pm 6.8(\text{stat}) \pm 9.3(\text{syst}) \mu\text{b}$. The results are unique in that they probe strong-interaction dynamics in a low- p_T regime unexplored in charm-meson production from proton-antiproton collisions. At higher transverse momentum, where previous measurements are available, the current measurements agree with earlier results [5]. While the individual measurement points lie within the band of theoretical uncertainty, the experimental spectrum is systematically shifted to high p_T values as compared with theory. This motivates the calculation of theoretical cross sections that include next-to-next-to-leading-order corrections, which are missing in current predictions thus contributing a large fraction of their uncertainty. Comparison of our results with higher-order predictions will further refine the shape of the theoretical cross section as a function of transverse momentum and reduce its uncertainty. The results are also helpful for understanding backgrounds in astrophysical ultra-high energy neutrino experiments, where the contributions from charm hadrons produced in the interaction of cosmic rays and atmospheric nuclei are the dominant background.

We thank the Fermilab staff and the technical staffs of the participating institutions for their vital contributions. This work was supported by the U.S. Department of Energy and National Science Foundation; the Italian Istituto Nazionale di Fisica Nucleare; the Ministry of Education, Culture, Sports, Science and Technology of Japan; the Natural Sciences and Engineering Research Council of Canada; the National Science Council of the Republic of China; the Swiss National Science Foundation; the A. P. Sloan

Foundation; the Bundesministerium für Bildung und Forschung, Germany; the Korean World Class University Program, the National Research Foundation of Korea; the Science and Technology Facilities Council and the Royal Society, United Kingdom; the Russian Foundation for

Basic Research; the Ministerio de Ciencia e Innovación, and Programa Consolider-Ingenio 2010, Spain; the Slovak R&D Agency; the Academy of Finland; the Australian Research Council (ARC); and the EU community Marie Curie Fellowship Contract No. 302103.

-
- [1] R. Gauld, J. Rojo, L. Rottoli, and J. Talbert, *J. High Energy Phys.* **11** (2015) 009; P. Lipari, *Astropart. Phys.* **1**, 195 (1993); L. Pasquali, M. Reno, and I. Sarcevic, *Phys. Rev. D* **59**, 034020 (1999); R. Enberg, M. H. Reno, and I. Sarcevic, *Phys. Rev. D* **78**, 043005 (2008); P. Gondolo, G. Ingelman, and M. Thunman, *Astropart. Phys.* **5**, 309 (1996); M. V. Garzelli, S. Moch, and S. Sigl, *J. High Energy Phys.* **10** (2015) 115; G. Gelmini, P. Gondolo, and G. Varieschi, *Phys. Rev. D* **61**, 036005 (2000).
- [2] B. Abbott *et al.* (D0 Collaboration), *Phys. Lett. B* **487**, 264 (2000); D. Acosta *et al.* (CDF Collaboration), *Phys. Rev. D* **65**, 052005 (2002).
- [3] P. Nason, S. Dawson, and R. K. Ellis, *Nucl. Phys.* **B327**, 49 (1989); **B335**, 260(E) (1990); W. Beenakker, W. L. Van Neerven, R. Meng, G. A. Schuler, and J. Smith, *Nucl. Phys.* **B351**, 507 (1991).
- [4] J. Binnewies, B. A. Kniehl, and G. Kramer, *Phys. Rev. D* **58**, 034016 (1998); M. Cacciari and P. Nason, *Phys. Rev. Lett.* **89**, 122003 (2002); M. Cacciari, arXiv:hep-ph/0407187.
- [5] D. Acosta *et al.* (CDF Collaboration), *Phys. Rev. Lett.* **91**, 241804 (2003).
- [6] B. Abelev *et al.* (ALICE Collaboration), *J. High Energy Phys.* **01** (2012) 128; *Phys. Lett. B* **718**, 279 (2012); *J. High Energy Phys.* **07** (2012) 191; R. Aaji *et al.* (LHCb Collaboration), *Nucl. Phys.* **B871**, 1 (2013); *J. High Energy Phys.* **03** (2016) 159; arXiv:1610.02230; arXiv:1702.00766.
- [7] We use the average of the inelastic cross sections reported in F. Abe *et al.* (CDF Collaboration), *Phys. Rev. D* **50**, 5535 (1994); C. Avila *et al.* (E811 Collaboration), *Phys. Lett. B* **445**, 419 (1999).
- [8] K. A. Olive *et al.* (Particle Data Group Collaboration), *Chin. Phys. C* **38**, 090001 (2014) and 2015 online update.
- [9] R. Blair *et al.* (CDF Collaboration), Report No. FERMI-LAB-PUB-96-390-E; T. Aaltonen *et al.* (CDF Collaboration), *Phys. Rev. D* **85**, 012009 (2012).
- [10] A. Sill, *Nucl. Instrum. Methods Phys. Res., Sect. A* **447**, 1 (2000).
- [11] T. Affolder *et al.*, *Nucl. Instrum. Methods Phys. Res., Sect. A* **526**, 249 (2004).
- [12] S. Klimentenko, J. Konigsberg, and T. M. Liss, Report No. Fermilab-FN-0741 (unpublished); D. Acosta *et al.*, *Nucl. Instrum. Methods Phys. Res., Sect. A* **494**, 57 (2002).
- [13] L. Marchese, Master's thesis, University of Naples Federico II, FERMILAB-MASTERS-2014-01, 2014.
- [14] We use the predictions from the calculations at next-to-leading order in the strong-interaction coupling and next-to-leading threshold logarithm by M. Cacciari and P. Nason, *J. High Energy Phys.* **09** (2003) 006 and updates at www.lpthe.jussieu.fr/~cacciari/fonll/fonllform.html.